ACS Energy LETTERS

http://pubs.acs.org/journal/aelccp

Dual Functional High Donor Electrolytes for Lithium–Sulfur Batteries under Lithium Nitrate Free and Lean Electrolyte Conditions

Ahmed Elabd,[#] Jiheon Kim,[#] Daniel Sethio,[#] Sangho Kang, Taemin Kang, Jang Wook Choi,* and Ali Coskun*

Cite This: https://doi.org/10.1021/acsenergylett.2c00874

Read Online

ACCESS | Metrics & More | Article Recommendations | Supporting Information

ABSTRACT: Electrolyte engineering is a highly promising strategy in lithium–sulfur batteries to increase the sulfur utilization and maintain a stable interface at the lithium metal anode for long-term cycling. Whereas high donor electrolytes can increase the solubility of polysulfides to promote the sulfur utilization and therefore operate under lean electrolyte conditions, their poor thermodynamic stability toward lithium metal anode causes uncontrolled decomposition at its interface and impair the cycle life severely. Here, we introduce a dual functional high donor electrolyte, 3-fluoropyridine (3-FPN), to simultaneously achieve high polysulfide solubility up to 1.5 M and compatibility with lithium metal. These features result in a high specific capacity of 1087.9 mAh g_{sulfur}^{-1} and robust cycling under a lean electrolyte condition of 7 $\mu L_{electrolyte}$ mg_{sulfur}^{-1} in the absence of $LiNO_3$. Remarkably, 3-FPN preserves stable cyclability even at a high areal sulfur loading of 8 mg_{sulfur} cm^{-2}, which opens a new avenue in advancing the electrolytes for lithium–sulfur batteries toward their high volumetric energy density and long cycle life.

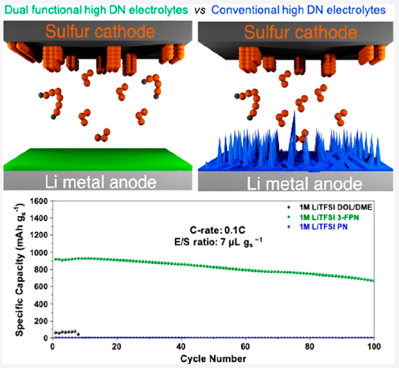

The rise of electric vehicles and grid energy storage systems fueled by growing environmental concerns has triggered a plethora of research activities on post-lithium-ion batteries (post-LIBs) with high energy densities, as the conventional LIBs are near saturating in terms of attainable specific energy.[1] In this direction, the lithium–sulfur (Li–S) battery has been considered to be a promising candidate because of the high gravimetric capacity of elemental sulfur (1675 $mAhg^{-1}$), high energy density of a cell (2600 Wh kg^{-1}), and the low cost and abundance of elemental sulfur.[2] In fact, elemental sulfur is one of the most abundant elements, produced as a byproduct of petroleum and natural gas refining.[3] Metallic Li separately brings its own advantage with respect to the high theoretical capacity. There are, however, still significant challenges that hamper the widespread use of Li–S cells: (1) the volume expansion of sulfur during discharge–charge process,[4] (2) the electrically insulating nature of elemental sulfur and its redox products, leading to sluggish kinetics and low sulfur utilization,[5,6] (3) a high electrolyte-to-sulfur ratio (E/S) (quantified in μL mg_{sulfur}^{-1}) > 20 μL mg_{sulfur}^{-1} that lowers the volumetric energy density,[7,8] and (4) lithium polysulfide (LiPS) shuttling[9,10] that harms the columbic efficiency in each cycle through parasitic reactions at the lithium metal surface.[11] Significant research efforts have been devoted to tackle these drawbacks, and the use of conductive sulfur-rich hosts,[12−14] redox mediators to mitigate shuttling effect,[15] passivation of lithium metal,[16] and introducing new high donor electrolytes for the operation of cells under lean electrolyte conditions are well-known approaches.[17−19]

The electrolyte stands pivotal in Li–S batteries as its amount largely determines the volumetric energy density of a cell. Along this direction, the E/S ratio is the main metric to consider, and the value below 10 μL mg_{sulfur}^{-1} is referred to as the lean electrolyte condition.[4,8] Unfortunately, lean electrolyte conditions are nontrivial to operate because of reduced ionic conductivity resulting from high viscosity and low solubility of LiPSs leading to poor sulfur utilization.[20] One effective approach to enable operation under lean conditions is the molecular design of electrolyte solvent such that it can solubilize sulfur redox species, promote disproportionation/dissociation of LiPS, and convert insoluble Li_2S. In this

Received: April 14, 2022
Accepted: July 1, 2022

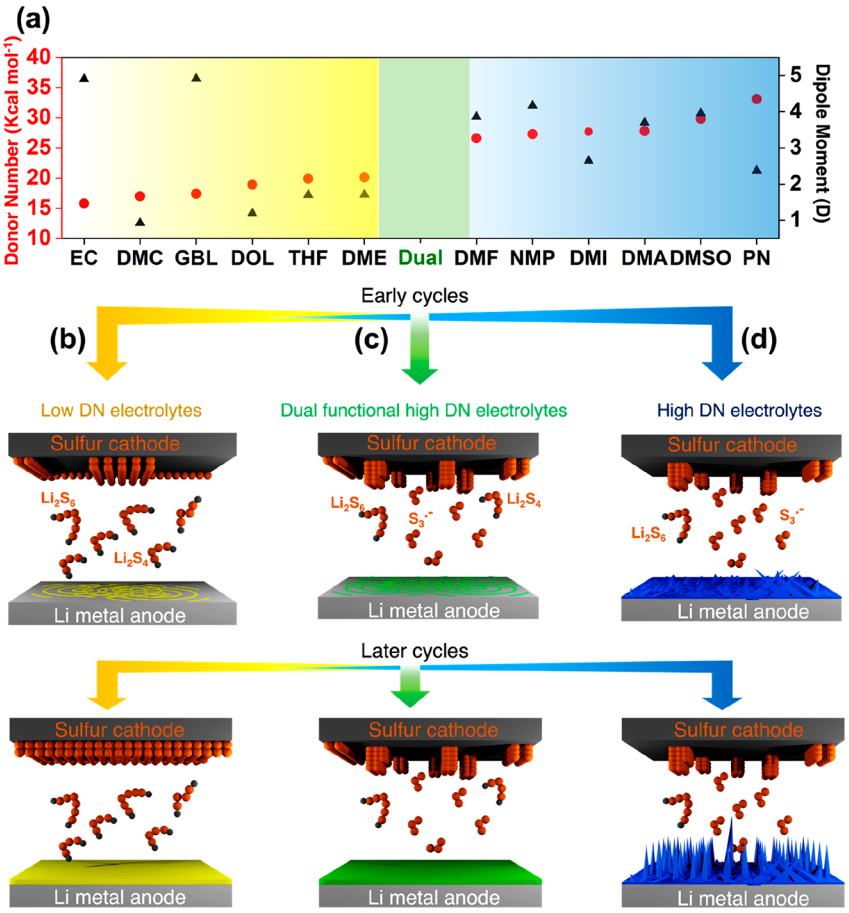

Figure 1. Effect of electrolyte donicity on the sulfur cathode, lithium metal anode, and LiPS redox mechanism. (a) Donor number (DN) and dipole moment (D) scales of various organic solvents. Schematic illustration of operating mechanisms in Li−S cells when the electrolytes with different donicities and functions are used: (b) low DN electrolyte, (c) dual functional high donor electrolyte, and (d) high DN electrolyte.

direction, solvents with a high Gutmann donor number (DN) are well aligned to promote the sulfur redox reactions and prevent sulfur cathode passivation compared to their low DN counterparts (Figure 1).[18,21−23] Recently, several high DN electrolytes based on dimethylacetamide (DMA, 27.8 kcal mol^{-1}),[23] *N*-dimethylformamide (DMF, 26.6 kcal mol^{-1}),[18] dimethyl sulfoxide (DMSO, 29.8 kcal mol^{-1}),[22] and 1,3-dimethyl-2-imidazolidinone (DMI, 29 kcal mol^{-1})[21] have been reported in contrast with the low donor systems such as 1,3-dioxolane (DOL, 18.9 kcal mol^{-1}) and 1,2-dimethoxyethane (DME, 20 kcal mol^{-1}) (Figure 1a,b).[24] The high donor electrolytes exhibit high initial discharge capacities under lean electrolyte conditions (Figure 1c,d), which is attributed to the unique features of high DN solvents: (i) high LiPS solubility greater than 1.5 M,[21] (ii) the ability to prevent the passivation of the cathode conductive surface by inducing 3D morphology of the final discharge product, Li_2S,[17,18] and (iii) the high density of donor electrons stabilizing sulfur-free radical, $S_3^{\bullet-}$, which acts as an intrinsic redox mediator to increase sulfur utilization.

Even with these clear advantages, employing high DN electrolytes in Li−S cells represents a complex paradox. With increasing donicity of the solvent, its reactivity toward lithium metal also increases in an uncontrolled manner, resulting in a short cycle life through unstable interface formation.[25] High donor anions such as NO_3^- [26,27] have long been used to passivate the lithium metal surface. Nevertheless, the low solubility of $LiNO_3$ in the electrolyte as well as gas evolution resulting from NO_3^- decomposition still present challenges.[18,26,28,29] Accordingly, controlling the electrolyte chemistry to impart dual functionality, high donicity, and passivation of Li metal in the absence of $LiNO_3$, is a rather promising approach. Unfortunately, the electrolytes reported to date can perform only one task; low DN electrolytes can only stabilize the Li metal anode surface whereas high DN electrolytes can only increase the LiPS solubility (Figure 1b,d). Hence, a new electrolyte chemistry that can perform the dual functions is highly desirable.

Schmulbach and co-workers studied the reactivity of alkali metals with pyridine (PN), noting the immediate formation of a coating layer through pyridine anchoring on the surface and subsequent dissolution of the metal layer.[30] More recently, pyridine derivatives have also been used as electrolyte additives to stabilize the Li metal surface by taking advantage of their anchoring via nitrogen atoms to the Li metal surface.[31−33] Moreover, pyridine possesses intrinsically high donicity (33.1 kcal mol^{-1})[34] so that pyridine and its derivatives are expected to facilitate high sulfur utilization. Therefore, modulating the donicity of PN through adding electronegative functional groups such as fluorine could be taken into consideration to weaken the high reactivity of PN toward the Li anode while retaining the high solubility of polysulfides. Notably, the

https://doi.org/10.1021/acsenergylett.2c00874
ACS Energy Lett. XXXX, XXX, XXX−XXX

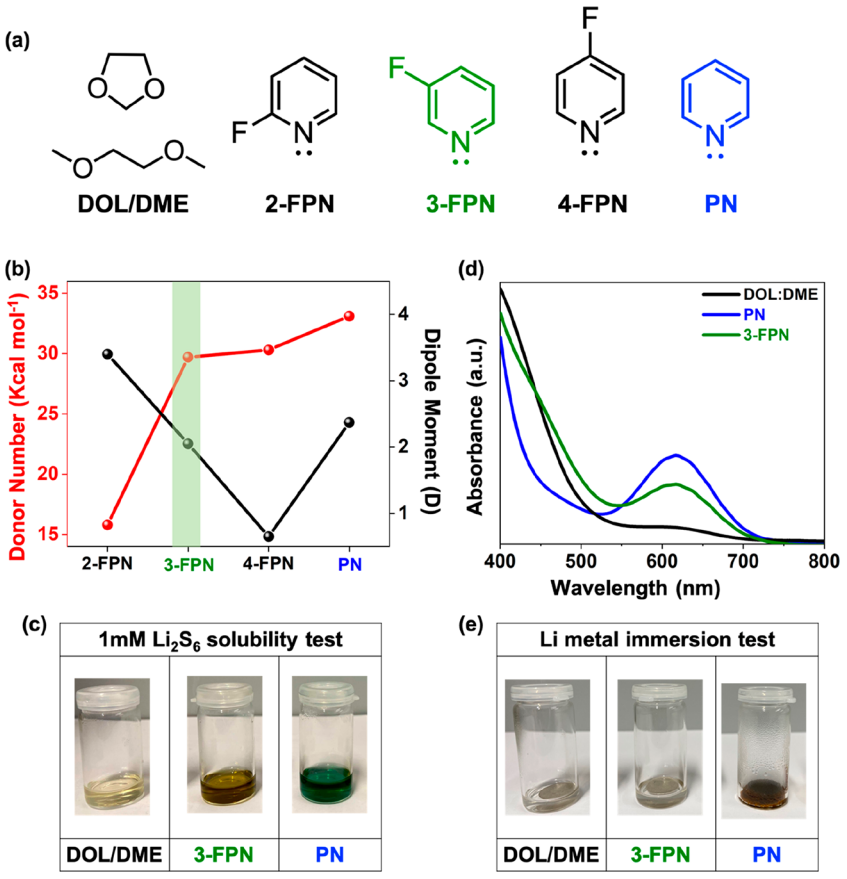

Figure 2. Chemical structures and physical properties of different solvents. (a) Chemical structures of 1,3-dioxolane, dimethoxyethane (DOL/DME), and pyridine (PN) and its −F substituted derivatives, namely, 2-FPN, 3-FPN, and 4-FPN. (b) DN numbers and dipole moments of 2-FPN, 3-FPN, 4-FPN, and PN. (c) Digital photographs of 1 mM Li_2S_6 solutions in DOL/DME, PN, and 3-FPN at room temperature. (d) UV−vis absorption spectra of 1 mM Li_2S_6 in DOL/DME, PN, and 3-FPN. (e) Digital photographs of lithium foil immersed in DOL/DME, 3-FPN, and PN after 30 min.

fluorination[35,36] of solvent, salt, and additive has been demonstrated to passivate Li metal anode by generating a homogeneous LiF-rich SEI layer and therefore mitigating the lithium dendrite growth.[37]

In this direction, we probed the effect of −F substitution of the PN ring at ortho, meta, and para positions (Figure 2a) on the PN's donicity. The DN and dipole moment values of 2-, 3-, and 4- fluoropyridine denoted as 2-FPN, 3-FPN, and 4-FPN were calculated using Dunning's aug-cc-pVTZ and Def2-SVPD basis set.[38,39] 3-FPN and 4-FPN displayed relatively high DNs of 29.7 and 30.3 kcal mol^{-1}, respectively, whereas that of 2-FPN was calculated to be only 15.8 kcal mol^{-1} (Figure 2b). Even though both 3- and 4-FPN showed similar DN values, we chose 3-FPN as an electrolyte solvent because 3-FPN is in the form of a liquid at room temperature whereas 4-FPN is isolated as a salt. The dipole moment of 4-FPN is also low (0.65 D). 3-FPN has additional advantages of good oxidation stability up to 4.0 V versus Li/Li^+ (Figure S1, Supporting Information), low density (1.13 $g.mL^{-1}$), and a high dipole moment of 2.05 D at 25 °C (Table S1). All of these properties allowed 3-FPN to achieve high LiPS solubility and passivate the Li metal anode compactly, jointly enabling the cycling of Li−S cells in a stable fashion under lean electrolyte conditions, i.e., E/S ratio $\lesssim 8\ \mu L\ mg_{sulfur}^{-1}$.

To evaluate the dual functionality of 3-FPN and verify its ability to operate under lean electrolyte conditions, LiPS solubility tests were performed for 3-FPN, PN, and DOL/DME (1:1 by volume). In line with their high donicity, both 3-FPN and PN were able to dissolve 1.5 M Li_2S_6 and form a clear solution without precipitation. In contrast, DOL/DME could not dissolve the same concentration of Li_2S_6 and the formation of precipitated sulfur species was clearly observed (Figure S2). It is noteworthy to mention that the high concentration of LiPS is directly related to higher sulfur utilization and thus the energy density of the corresponding cell. To evaluate LiPS stability in different solvents, 1 mM Li_2S_6 solutions were prepared by reacting equimolar amounts of elemental sulfur and Li_2S in 3-FPN, PN, and DOL/DME. The results were in good agreement with the physical properties of solvents (Table S1) such as donicity and dipole moment. 3-FPN and PN as high DN solvents formed dark yellowish-green colored solutions, which indicate the existence of sulfur radicals $S_3^{\bullet-}$,[21] whereas DOL/DME with low donicity formed a colorless solution (Figure 2c). The speciation of LiPS (disproportionation and dissociation reactions) was further elucidated (Figure 2d) by ultraviolet−visible (UV−vis) spectroscopy analysis. PN exhibited a peak at 618 nm with the highest intensity corresponding to sulfur radicals $S_3^{\bullet-}$ originating from the disproportionation reaction of S_6^{2-}.[31] The greater amount of stabilized $S_3^{\bullet-}$ in the case of PN is attributed to its higher donicity compared to 3-FPN.[17] Consistent with the literature,[18] DOL/DME did not display any discernible peaks except for the one at 420 nm, which is an indication of the existence of S_4^{2-}.[26] Interestingly, 3-FPN

https://doi.org/10.1021/acsenergylett.2c00874
ACS Energy Lett. XXXX, XXX, XXX−XXX

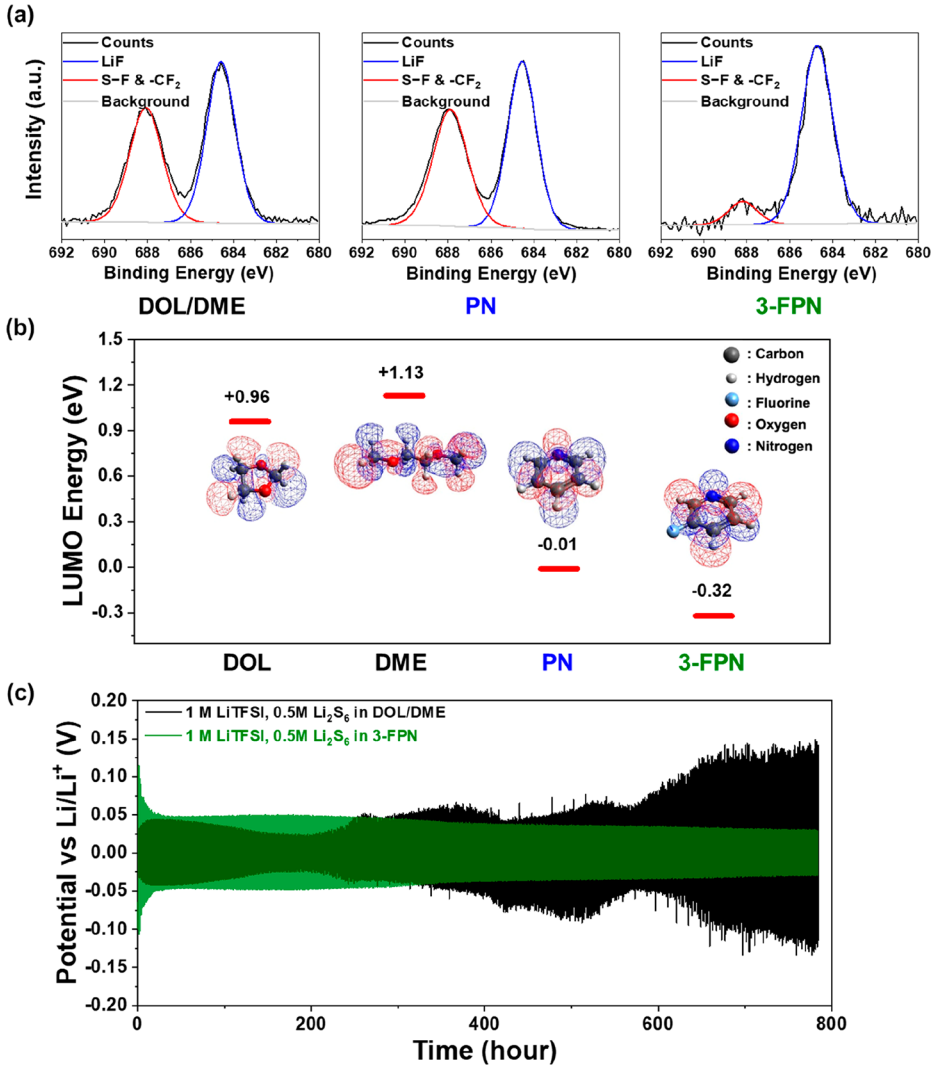

Figure 3. Understanding the impact of different solvents on the passivation of the Li metal surface. (a) F 1s XPS profiles of the SEI layers in the presence of different electrolytes, 1 M LiTFSI-DOL/DME, 1 M LiTFSI-PN, and 1 M LiTFSI-3-FPN, after one cycle of Li plating and stripping at a capacity of 0.1 mAh cm^{-2} and a current density of 0.1 mA cm^{-2}. (b) Calculation of LUMO energy levels of DOL, DME, PN, and 3-FPN. (c) Cycling performance of Li−Li symmetric cells of 1 M LiTFSI and 0.5 M Li_2S_6 in DOL/DME and 3-FPN at a capacity of 0.5 mAh cm^{-2} and a current density of 0.5 mA cm^{-2}.

exhibited the substantial presence of all of S_6^{2-}, S_4^{2-}, and $S_3^{\bullet-}$ species, as evidenced by the broad absorption bands located at 420, 475, and 618 nm, respectively, thus revealing the profound impact of solvents on the distribution of sulfur species.

The conventional high DN solvents suffer from their high chemical reactivity toward metallic lithium, thus severely limiting their practical feasibility in Li−S cells. Accordingly, we performed immersion tests of the lithium foil to probe the reactivity of 3-FPN, PN, and DOL/DME (Figure 2e). One milliliter of each solvent was transferred to a vial and lithium discs were immersed for 30 min. As expected, the DOL/DME mixture was stable toward lithium metal because of its low donicity.[11] In line with the earlier findings, PN showed a very high reactivity toward lithium metal, leading to solvent consumption because of the uncontrolled decomposition of PN at the surface. However, 3-FPN showed a remarkable stability toward lithium metal, sustaining an intact smooth surface without any severe reaction, reflecting its controlled reactivity through −F substitution despite its high donicity.

The corresponding electrolytes were prepared by dissolving lithium bis(trifluoromethane)sulfonimide (LiTFSI) in the respective solvents and are referred to as 1 M LiTFSI-PN, 1 M LiTFSI-3-FPN, and 1 M LiTFSI-DOL/DME, respectively. To probe the chemical composition of SEI on the Li metal surface, X-ray photoelectron spectroscopy (XPS) analysis was performed after one cycle of Li plating and stripping with an areal capacity of 0.5 mAh cm^{-2} at a current density of 0.5 mA cm^{-2}. The formation of an inorganic-rich SEI layer with a high LiF content has been shown to be beneficial in effectively stabilizing Li metal anode by alleviating Li dendrite growth and parasitic reactions with liquid electrolyte.[37] Accordingly, we focused on the F 1s and Li 1s bands to detect the LiF content in the SEI (Figure 3a). For the F 1s branch, all electrolytes manifested peaks at 684.8 and 688.7 eV, which could be correlated to LiF and S−F and C−F bonds, respectively, originating from the decomposition of lithium bis(trifluoromethane)sulfonimide (LiTFSI) and/or fluorinated solvents. The formation of LiF was further proven by the peak at 55.6 eV in the Li 1s branch (Figure S3).[37] Intriguingly, PN

https://doi.org/10.1021/acsenergylett.2c00874
ACS Energy Lett. XXXX, XXX, XXX−XXX

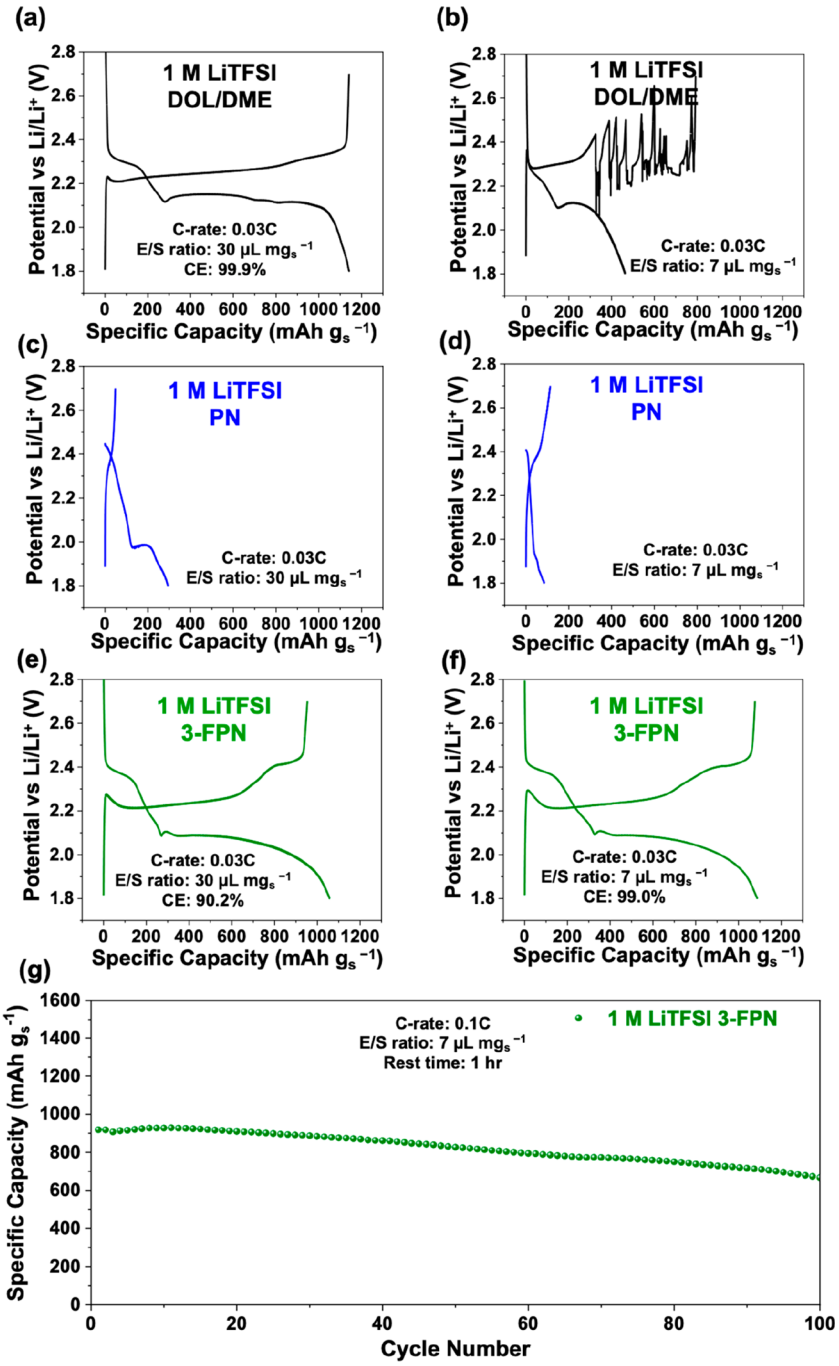

Figure 4. Electrochemical performance of different electrolytes under flooded and lean conditions. First discharge−charge profiles of Li−S cells at a scan rate 0.03C (1C = 1675 mA g^{-1}) with different electrolytes under flooded conditions with an E/S ratio of 30 $\mu L_{electrolyte}$ mg_{sulfur}^{-1}: (a) 1 M LiTFSI-DOL/DME, (b) 1 M LiTFSI-PN, and (c) 1 M LiTFSI-3-FPN. First discharge−charge profiles of Li−S cells at a scan rate 0.03C (1C = 1675 mA g^{-1}) with different electrolytes under lean conditions with an E/S ratio of 7 $\mu L_{electrolyte}$ mg_{sulfur}^{-1}: (d) 1 M LiTFSI-DOL/DME, (e) 1 M LiTFSI-PN, and (f) 1 M LiTFSI-3-FPN. (g) Cycling performance of 1 M LiTFSI-PN, 1 M LiTFSI-3-FPN, and 1 M LiTFSI-DOL/DME electrolytes with an areal sulfur loading of 1.0 mg_{sulfur} cm^{-2} and E/S ratio of 7 $\mu L_{electrolyte}$ mg_{sulfur}^{-1} at 0.1C scan rate in the potential range 1.8−2.7 V.

and DOL/DME showed relatively high yet comparable intensities of both LiF and S−F and C−F peaks, whereas in the case of 3-FPN, the LiF peak was far more dominant over the other two peaks. This observation is ascribed to the ability of 3-FPN to supply fluorine in the formation of the SEI layer beyond the capability of traditional high DN solvents.

To further elaborate on the reactivity of the solvents toward Li metal, we calculated the lowest unoccupied molecular orbital (LUMO) levels to elucidate the reduction priority of DOL, DME, 3-FPN, and PN (Figure 3b). Because of the electronegativity of the fluorine atom, 3-FPN showed the lowest LUMO level of −0.32 eV followed by PN (0.01), DOL (+0.09), and DME (+0.096 eV). The evaluation of LUMO levels gives a clue to the enhanced formation of LiF in the case of 3-FPN; the vulnerability of 3-FPN to reduction and its

https://doi.org/10.1021/acsenergylett.2c00874
ACS Energy Lett. XXXX, XXX, XXX−XXX

surface anchoring increase the chance of providing fluorine toward reacting with metallic Li.

The effect of 3-FPN on the Li metal interface was assessed using LilLi symmetric cells in the absence of $LiNO_3$. To simulate a practical Li−S cell in which the polysulfide catholyte is formed and shuttles, the analysis was performed using 10 μL of 1 M LiTFSI and 0.5 M Li_2S_6 at a current density of 0.5 mA cm^{-2} with an areal capacity of 0.5 mAh cm^{-2} (Figure 3c) and the magnified views of the Li potential profiles LilLi symmetric cells are presented to discern the overpotential difference (Figure S4). The dual functionality of 3-FPN was clearly observed over extended cycling, for which DOL/DME showed an overpotential increase up to 150 mV upon cycling, suggesting severe parasitic side reactions. In the case of 3-FPN electrolyte, an initial increase in the overpotential was observed, which is attributed to the anchoring and subsequent reduction of 3-FPN on the lithium metal surface, leading to the formation of a LiF-rich SEI layer. The impact of passivation of the Li metal surface by 3-FPN was revealed by the stable long cycling over 750 h with a stable polarization of 30 mV, which indicates the formation of a robust SEI layer and highly reversible Li plating/stripping even in the absence of $LiNO_3$. Notably, 3-FPN is the first high donor solvent, which is capable of passivating the Li metal surface over 750 cycles without $LiNO_3$.

The electrochemical performance of 1 M LiTFSI-PN, 1 M LiTFSI-3-FPN, and 1 M LiTFSI-DOL/DME electrolytes was assessed in Li−S full cells using galvanostatic charge−discharge tests. These experiments were performed under flooded (30 μL mg_{sulfur}^{-1}) and lean electrolyte conditions (7 μL mg_{sulfur}^{-1}) by employing sulfur cathodes with an areal loading of 1.0 mg_{sulfur} cm^{-2} at a scan rate of 0.03C (1C = 1675 mA g^{-1}). The cells based on 1 M LiTFSI-3-FPN and 1 M LiTFSI-DOL/DME electrolytes under flooded conditions exhibited highly reversible charge−discharge profiles with specific capacity values >1000 mAh g_{sulfur}^{-1} and high initial columbic efficiency (ICE) over 90% (Figure 4a,e) contrasting to the electrochemical performance of PN, which delivered a rather low specific capacity <350 mAh g_{sulfur}^{-1} (Figure 4c) because of its high chemical reactivity toward lithium metal. Under the lean electrolyte conditions, however, only the cell based on 1 M LiTFSI-3-FPN maintained an exceptional specific capacity of 1087.9 mAh g_{sulfur}^{-1} (Figure 4f) along with a reversible charge−discharge plateau and the ICE of 99.0%. In stark contrast, the cells based on 1 M LiTFSI-PN and 1 M LiTFSI-DOL/DME failed to operate under the lean electrolyte conditions (Figure 4b,d) because of the low LiPS solubility in the case of DOL/DME and the high chemical reactivity toward Li metal in the case of PN, thus leading to unstable charge−discharge profiles. To probe the long cycling stability of 3-FPN, the galvanostatic tests were carried out with an areal loading of 1.0 mg_{sulfur} cm^{-2} at 0.1C and the E/S value of 7 μL mg_{sulfur}^{-1} (Figure 4g). Notably, 3-FPN exhibited a superior average discharge capacity of 792.7 mAh g_{sulfur}^{-1} over 100 cycles with a good capacity retention outperforming previously reported high donor electrolytes under lean conditions.[7,17−19,21−23] On the contrary, DOL/DME and PN failed to deliver any tangible specific capacity in the first cycle. Whereas the CE of 3-FPN saturated near 120% over 100 cycles (Figure S5a), those of DOL/DME and PN were unstable such that they increased over 200% only after a few cycles (Figure S5b,c). The abnormal CE values indicate a higher charge capacity than discharge capacity. The origins of this phenomenon are mostly attributed to the inevitable overcharging involving polysulfide shuttling and the formation of sulfur concentration gradient in the catholyte.[18,25,40] Nevertheless, 3-FPN was able to alleviate these shortcomings to a certain extent and achieve stable cycling. Further analysis of CE and specific capacity of 3-FPN was performed (Figure S6) during cycling at a higher C-rate of 0.3C and with an E/S ratio of 7 μL mg_{sulfur}^{-1}. The cell based on 3-FPN electrolyte exhibited an ICE of 68.1% and stabilized CE near 100% over 100 cycles along with an initial discharge capacity of 572.8 mAh g_{sulfur}^{-1} and a moderate capacity retention. These results showed the feasibility of pyridine-based solvents to realize the ideal balance between stable CE and higher specific capacity under the lean electrolyte conditions. To further optimize the CE and capacity retention at higher C-rates, the effect of $LiNO_3$ was assessed by adding 0.2 M $LiNO_3$ to 1 M LiTFSI-3-FPN and 1 M LiTFSI-DOL/DME. The corresponding galvanostatic charge−discharge tests were performed at 7 μL mg_{sulfur}^{-1} by employing sulfur cathodes with an areal loading of 1.0 mg_{sulfur} cm^{-2} at a scan rate of 0.03C (1C = 1675 mA g^{-1}). Notably, 3-fluoropyridine solvent delivered ideal charging/discharging profiles with/without $LiNO_3$, whereas DOL/DME showed unstable charging profiles originating from its low DN and limited solubility of LiPS regardless of the presence of $LiNO_3$ (Figure S7). Moreover, the long-term cycling test of 3-fluoropyridine in the presence of $LiNO_3$ at 0.1C exhibited a stable CE close to 100% and a capacity retention of 92% after 50 cycles. In stark contrast, DOL/DME showed unstable capacity retention, an aggravated CE over 600% and cell failure after 20 cycles with and without $LiNO_3$, once again, because of the poor solubility of LiPS (Figure S8). We note that the addition of $LiNO_3$ enhanced the CE and capacity retention of both electrolytes to some extent. Additionally, we further evaluated both electrolytes with $LiNO_3$ at a higher C-rate of 0.3C that might be relevant for practical applications. Remarkably, 3-fluoropyridine delivered a decent capacity retention of 89.6% after 100 cycles and a stable CE near 100% with an E/S ratio of 7 $\mu L_{electrolyte}$ mg_{sulfur}^{-1} (Figure S9). Scanning electron microscopy (SEM) analysis was conducted to examine Li deposition after 10 cycles with and without $LiNO_3$ additive in the ether-based and 3-FPN-based electrolytes at a current density of 0.1 mA cm^{-2}. As shown in Figure S10a, the 1 M LiTFSI-DOL/DME cell displayed needle-like microstructures, typical morphology of Li dendrites that grow uncontrollably because of the poor Li plating originating from the high interfacial resistance. In the presence of $LiNO_3$, the 1 M LiTFSI-DOL/DME cell appeared (Figure S10b) to form a chunky Li with a large granular size. However, more chunky Li with much larger granular size was observed in the case of 1 M LiTFSI-3-FPN (Figure S10c) and 1 M LiTFSI-0.2 M $LiNO_3$-3-FPN (Figure S10d) electrolytes. Whereas $LiNO_3$ significantly improved the morphology in DOL/DME, in the case of 3-FPN, the effect was not as evident because of the ability of 3-FPN solvent to stabilize the Li metal surface.

We also obtained the XPS depth profiles for 1 M LiTFSI-3-FPN and 1 M LiTFSI-0.2 M $LiNO_3$-3-FPN to evaluate the effect of these electrolytes on the SEI composition (Figure S11). Interestingly, the 1 M LiTFSI-3-FPN electrolyte showed nearly constant LiF content along the depth, proving that LiF is homogeneously distributed within the SEI. We also observed increasing Li_2O content with etching time. These data clearly suggest an inorganic-rich SEI formation in the case of 3-FPN. In the presence of $LiNO_3$, whereas we observed a massive

https://doi.org/10.1021/acsenergylett.2c00874
ACS Energy Lett. XXXX, XXX, XXX−XXX

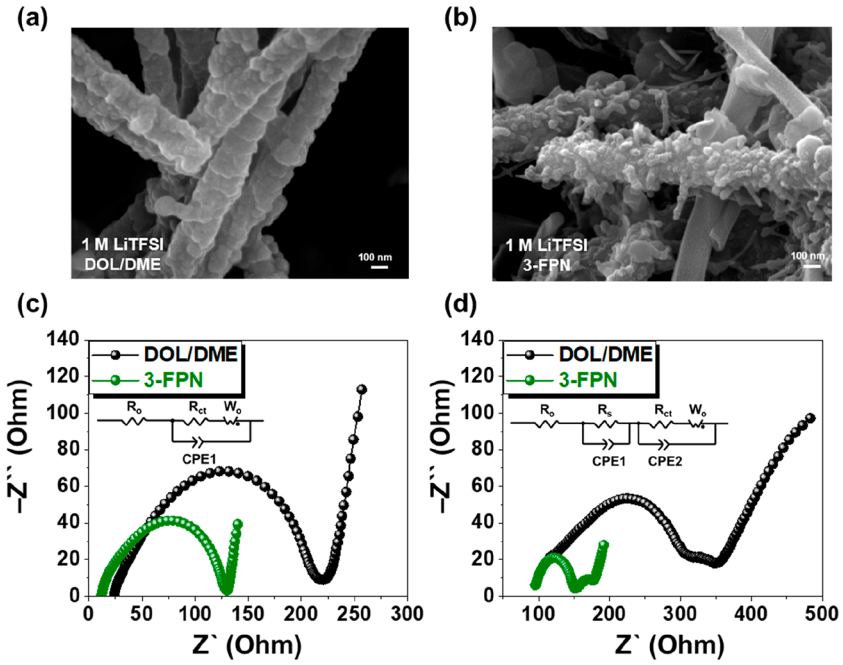

Figure 5. Characterization of Li_2S deposition on the sulfur cathode surface in different electrolytes. SEM images of the Li_2S electrodeposition on the sulfur cathode with 30 μL of catholyte composed of 0.08 M Li_2S_6 and 1 M LiTFSI in (a) DOL/DME and (b) 3-FPN solvents. The surface morphologies of the Li_2S deposits on the cathode surface were investigated after discharging to 1.8 V at 0.03C. EIS profiles of 1 M LiTFSI-DOL/DME and 1 M LiTFSI-3-FPN electrolytes in Li−S cells (c) before cycling and (d) after 10 cycles. EIS analysis was conducted in the frequency range 1 MHz to 0.1 Hz with an amplitude of 10 mV at the open circuit potential.

decrease in the LiF content, Li_2O was found to be constant along the depth. Considering the XPS results, we can infer that the 3-FPN and 3-FPN/$LiNO_3$ induced an inorganic-rich, Li-conductive (as inferred by the low R_{ct} as discussed below) SEI layer on the Li metal anodes upon decomposition. The series of results can be comprehensively understood in such a way that 3-FPN itself was able to stabilize the SEI layer by forming a LiF-rich SEI whereas the $LiNO_3$ addition promoted higher relative Li_2O content to LiF because of the competitive decomposition between 3-FPN and $LiNO_3$.[41,42] Along this context, CE close to 100% in the presence of $LiNO_3$ points to its role toward better stabilizing the SEI. These observations are also in agreement with the SEM and electrochemical analysis results.

The morphology of Li_2S provides critical information on its nucleation and growth mechanism, which have a profound impact on the surface passivation of sulfur cathode. High DN electrolytes promote the growth of 3D Li_2S particles by increasing the nucleation barrier and reducing the nucleation density, thus preserving the conductive surface of the cathode. However, low DN solvents favor 2D film growth with slow reaction kinetics, resulting in the formation of an insulating layer on the cathode surface.[17,21,26] In this direction, scanning electron microscopy (SEM) analysis was performed for the cathodes in their discharged states to investigate Li_2S electrodeposition behavior in the presence of a catholyte containing DOL/DME or 3-FPN, 1 M LiTFSI, and 0.08 M Li_2S_6. The cathode morphology in DOL/DME exhibited predominantly micron sized, 0.2−0.3 μm, 2D plates/sheets, which points to the lateral nucleation and continuous growth of insulating Li_2S, thus causing cathode passivation (Figure 5a). In stark contrast, 3-FPN enabled the nucleation and growth of 3D Li_2S granules with an average size of 100 nm (Figure 5b), which can alleviate surface passivation and promote facile charge transfer. These results clearly reflect that the different Li_2S morphologies between the two electrolytes originates from their distinct donicity and resulting nucleation mechanisms.

We also performed electrochemical impedance spectroscopy (EIS) analysis for the cells based on 1 M LiTFSI-DOL/DME and 1 M LiTFSI-3-FPN (Figure 5c,d). The corresponding Nyquist plots before cycling exhibited a semicircle at the high and medium frequency regimes and a subsequent inclined line at the low frequency regime. The intercept on the real axis at high frequency indicates the bulk resistance (R_o) of the cell, which consists of the electrode and the electrolyte resistance.[43] The semicircle at the high-to-medium frequency regime is indicative of the interface charge-transfer resistance (R_{ct}), whereas the inclined line at the low frequency regime is attributed to the Warburg impedance (W_o) associated with Li-ion diffusion.[44] Before cycling, the cell with 1 M LiTFSI-3-FPN electrolyte exhibited a R_o value of 11.6 Ω, which is about half of that of DOL/DME (23.5 Ω). Moreover, the same trend was also observed in the charge-transfer resistance, where the cell with 1 M LiTFSI-3-FPN electrolyte showed a lower R_{ct} value of 118.7 Ω compared to that of DOL/DME (199.5 Ω). After 10 cycles, the semicircles were divided into two smaller circles, where the first circle in the high frequency regime is attributed to the deposition of Li_2S/Li_2S_2 layer onto the cathode,[45] the so-called surface resistance (R_s), whereas the circle in the medium frequency regime corresponds to the R_{ct} of the cathode.[46−48] The cell with 1 M LiTFSI-3-FPN electrolyte exhibited R_o, R_s, and R_{ct}, values of 91.8, 61.7, and 16.5 Ω, respectively, whereas those of the cell with 1 M LiTFSI-DOL/DME were found to be 105.7, 227.0, and 20.28 Ω, respectively. The relatively smaller R_s and R_{ct} values of 3-FPN cell corroborate its superior kinetics related to the 3D Li_2S deposition in the cathode and stable SEI layer formation

https://doi.org/10.1021/acsenergylett.2c00874
ACS Energy Lett. XXXX, XXX, XXX−XXX

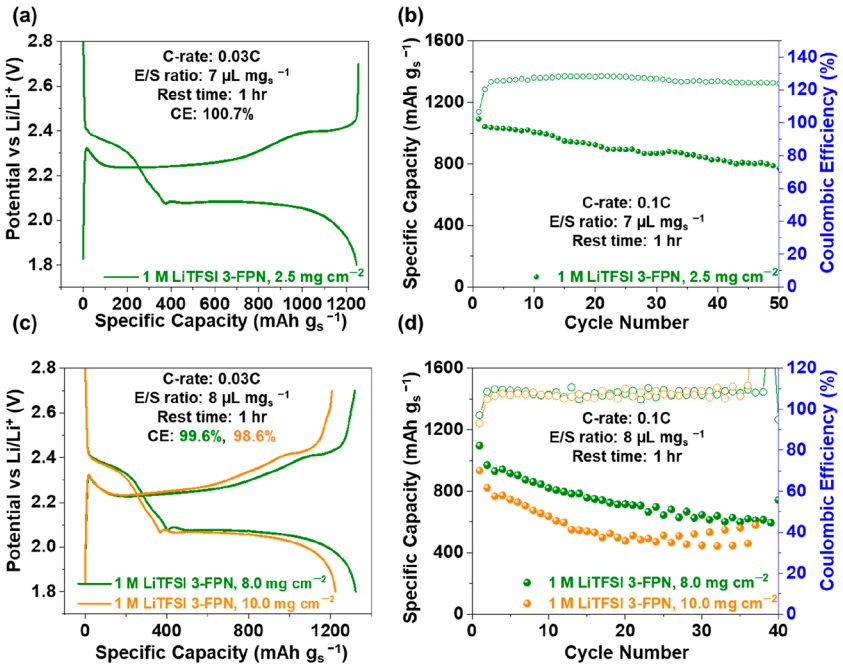

Figure 6. Electrochemical characterization of 1 M LiTFSI-3-FPN electrolyte at high areal sulfur loadings. (a) Initial discharge−charge profiles at 0.03C in the potential range 1.8−2.7 V vs Li/Li$^+$ and (b) cycling test at 0.1C with the areal sulfur loading of 2.5 mg$_{sulfur}$ cm^{-2} and E/S ratio of 7 μL$_{electrolyte}$ mg$_{sulfur}$$^{-1}$. The 16 π C/S electrodes were fabricated with carbon black and PvdF. (c) Voltage profiles at 0.03C and (d) cycling performance at 0.1 C with areal sulfur loadings of 8.0 (green) and 10.0 mg$_{sulfur}$ cm^{-2} (orange) and E/S ratio of 8 μL$_{electrolyte}$ mg$_{sulfur}$$^{-1}$.

on the Li metal anode surface. Furthermore, the sulfur redox kinetics of 1 M LiTFSI-3-FPN electrolyte in comparison with a conventional high donor electrolyte, 1 M LiTFSI-DMA, and a low donor electrolyte, 1 M LiTFSI-DOL/DME was assessed using a potentiostatic reaction test (Figure S12). The potentiostatic reaction tests were conducted in Li−S full cells with different electrolytes at an E/S ratio of 7 μL mg$_{sulfur}$$^{-1}$ and an areal sulfur loading of 1.0 mg$_{sulfur}$ cm^{-2}. The cells were galvanostatically discharged at 0.1C to 2.10 V, followed by a potential shift to 2.05 V, at which the output current was monitored during the nucleation and growth of Li_2S_2/Li_2S. By application of a constant discharge potential of 2.05 V for 25000 s, the output surging current is assigned to Li_2S_2/Li_2S nucleation and the subsequent current reflects the growth of nucleated Li_2S_2/Li_2S, which could identify the difference in sulfur redox kinetics between low and high donor electrolytes.[49,50] The reaction kinetics of nucleation and growth of Li_2S is closely related to solvent donacity and polysulfide solubility. Generally, with increasing solvent donacity; the solubility of polysulfides increases, the conversion reaction overpotential increases, and the reaction kinetics of sulfur slows down, which are all collectively reflected in the potentiostatic curve.[51] One molar LiTFSI-DOL/DME showed a current decay over time because of its limited ability to solubilize Li_2S_2/Li_2S, whereas 1 M LiTFSI-DMA presented a severe current drop because of the aggravated overpotential and uncontrolled reactivity toward Li metal. In the case of 1 M LiTFSI-3-FPN, even with a high donacity, it still realized a current density comparable to that of 1 M LiTFSI-DOL/DME because of its dual-functionality. More importantly, the corresponding specific capacity representing the total amount of conversion reaction indicates that 1 M LiTFSI-3-FPN is superior to 1 M LiTFSI-DOL/DME, which suggests that the high density of donor electrons stabilizes sulfur-free radical $S_3^{\bullet-}$, which is acting as an intrinsic redox mediator to increase sulfur utilization while preserving the compatibility with the Li metal.

In an effort to test the electrochemical performance of 1 M LiTFSI-3-FPN electrolyte under practical Li−S battery conditions, we performed electrochemical tests at high sulfur loadings under lean electrolyte conditions. The areal sulfur loading was first increased to 2.5 mg$_{sulfur}$ cm^{-2}, and the E/S ratio was set to 7 μL mg$_{sulfur}$$^{-1}$. Remarkably, the galvanostatic charge−discharge test exhibited an ideal charge−discharge profile with an excellent reversibility and a significant specific capacity of 1247.4 mAh g$_{sulfur}$$^{-1}$ (Figure 6a). Hence, the cycling performance test at 0.1C was carried out to further evaluate the 1 M LiTFSI-3-FPN electrolyte for long cycling. The cell with 1 M LiTFSI-3-FPN electrolyte sustained a significant capacity retention of 70.7% after 50 cycles with a stable CE around 120% (Figure 6b). Encouraged by these findings, further analysis of 1 M LiTFSI-3-FPN electrolyte was performed at high areal sulfur loadings of 8.0 and 10.0 mg$_{sulfur}$ cm^{-2} in pellet cells with an E/S ratio of 8 μL mg$_{sulfur}$$^{-1}$. We observed highly reversible charge−discharge profiles at 0.03C for both 8.0 and 10.0 mg$_{sulfur}$ cm^{-2} with substantial specific capacities of 1322.8 and 1224.8 mAh g$_{sulfur}$$^{-1}$, respectively (Figure 6c). The cell with 8.0 mg$_{sulfur}$ cm^{-2} exhibited relatively stable cycling over 40 cycles, whereas the one with 10.0 mg$_{sulfur}$ cm^{-2} showed capacity fluctuation after 30 cycles (Figure 6d). Interestingly, both cells showed steady CEs around 108% over the course of cycling. We emphasize that the observed cycling performance at this lean electrolyte condition is not trivial for the given high levels of sulfur loading, and DOL/DME does not operate at all in these electrolyte and sulfur loading conditions. Moreover, these performance metrics surpass (Table S2) all the previously reported high donor electrolytes in Li−S batteries.

https://doi.org/10.1021/acsenergylett.2c00874
ACS Energy Lett. XXXX, XXX, XXX−XXX

In summary, we introduced a new class of high donor solvents capable of simultaneously achieving high polysulfide solubility up to 1.5 M and compatibility with the lithium metal anode, enabling exceptional cycling stability at high areal sulfur loadings under lean electrolyte conditions even in the absence of $LiNO_3$. The incorporation of fluorine atom onto the pyridine ring not only properly controlled the donicity of 3-FPN but also facilitated the formation of a LiF-rich, stable SEI layer on the Li metal surface. This dual functional high donor solvent sets a new benchmark for the design of electrolytes targeting practical Li−S batteries.

■ ASSOCIATED CONTENT

Supporting Information

The Supporting Information is available free of charge at https://pubs.acs.org/doi/10.1021/acsenergylett.2c00874.

Experimental details, linear sweep voltammetry curves, optical and SEM images, XPS spectra, potential profiles, Coulombic efficiency, cycling performance, discharge−charge profiles, potentiostatic reaction curves, table of physical properties of the tested solvents, and summary of the electrochemical performances (PDF)

■ AUTHOR INFORMATION

Corresponding Authors

Jang Wook Choi − *Department of Chemistry, University of Fribourg, Fribourg 1700, Switzerland;* orcid.org/0000-0001-8783-0901; Email: jangwookchoi@snu.ac.kr

Ali Coskun − *School of Chemical and Biological Engineering, Department of Materials Science and Engineering, and Institute of Chemical Processes, Seoul National University, Gwanak-gu, Seoul 08826, Republic of Korea;* orcid.org/0000-0002-4760-1546; Email: ali.coskun@unifr.ch

Authors

Ahmed Elabd − *Department of Chemistry, University of Fribourg, Fribourg 1700, Switzerland;* orcid.org/0000-0001-9570-1018

Jiheon Kim − *School of Chemical and Biological Engineering and Institute of Chemical Processes, Seoul National University, Gwanak-gu, Seoul 08826, Republic of Korea*

Daniel Sethio − *Department of Chemistry, BMC Uppsala University, 751 23 Uppsala, Sweden;* orcid.org/0000-0002-8075-1482

Sangho Kang − *School of Chemical and Biological Engineering and Institute of Chemical Processes, Seoul National University, Gwanak-gu, Seoul 08826, Republic of Korea*

Taemin Kang − *School of Chemical and Biological Engineering and Institute of Chemical Processes, Seoul National University, Gwanak-gu, Seoul 08826, Republic of Korea*

Complete contact information is available at: https://pubs.acs.org/10.1021/acsenergylett.2c00874

Author Contributions

#A.E. and J.K. contributed equally to this work. D.S. performed the computational analysis.

Notes

The authors declare the following competing financial interest(s): University of Fribourg, Switzerland, and Seoul National University, Republic of Korea, are in the process of filing a patent application for the solvents and electrolytes described in this manuscript.

■ ACKNOWLEDGMENTS

A.C. acknowledges the support from Swiss National Science Foundation (SNF) for funding of this research (200021-188572). J.W.C. acknowledges the support from the National Research Foundation of Korea (NRF) (NRF-2021R1A2B5B03001956), the Technology Innovation Program (20012341) funded by the Ministry of Trade, Industry & Energy (MOTIE) of Korea, and generous support from the Institute of Engineering Research (IOER) and Interuniversity Semiconductor Research Center (ISRC) at Seoul National University.

■ REFERENCES

(1) Fang, R.; Zhao, S.; Sun, Z.; Wang, D.-W.; Cheng, H.-M.; Li, F. More Reliable Lithium-Sulfur Batteries: Status, Solutions and Prospects. *Adv. Mater.* **2017**, *29* (48), 1606823.

(2) Manthiram, A.; Fu, Y.; Chung, S.-H.; Zu, C.; Su, Y.-S. Rechargeable Lithium−Sulfur Batteries. *Chem. Rev.* **2014**, *114* (23), 11751−11787.

(3) Rauchfuss, T. Under sulfur's spell. *Nat. Chem.* **2011**, *3* (8), 648.

(4) Bhargav, A.; He, J.; Gupta, A.; Manthiram, A. Lithium-Sulfur Batteries: Attaining the Critical Metrics. *Joule* **2020**, *4* (2), 285−291.

(5) He, J.; Manthiram, A. A review on the status and challenges of electrocatalysts in lithium-sulfur batteries. *Energy Storage Mater.* **2019**, *20*, 55−70.

(6) Ren, W.; Ma, W.; Zhang, S.; Tang, B. Recent advances in shuttle effect inhibition for lithium sulfur batteries. *Energy Storage Mater.* **2019**, *23*, 707−732.

(7) Kong, L.; Yin, L.; Xu, F.; Bian, J.; Yuan, H.; Lu, Z.; Zhao, Y. Electrolyte solvation chemistry for lithium−sulfur batteries with electrolyte-lean conditions. *J. Energy Chem.* **2021**, *55*, 80−91.

(8) Zhao, M.; Li, B.-Q.; Peng, H.-J.; Yuan, H.; Wei, J.-Y.; Huang, J.-Q. Lithium−Sulfur Batteries under Lean Electrolyte Conditions: Challenges and Opportunities. *Angew. Chem., Int. Ed.* **2020**, *59* (31), 12636−12652.

(9) Huang, L.; Li, J.; Liu, B.; Li, Y.; Shen, S.; Deng, S.; Lu, C.; Zhang, W.; Xia, Y.; Pan, G.; et al. Electrode Design for Lithium−Sulfur Batteries: Problems and Solutions. *Adv. Funct. Mater.* **2020**, *30* (22), 1910375.

(10) Pang, Q.; Liang, X.; Kwok, C. Y.; Nazar, L. F. Advances in lithium−sulfur batteries based on multifunctional cathodes and electrolytes. *Nat. Energy* **2016**, *1* (9), 16132.

(11) Hong, H.; Che Mohamad, N. A. R.; Chae, K.; Marques Mota, F.; Kim, D. H. The lithium metal anode in Li−S batteries: challenges and recent progress. *J. Mater. Chem.* **2021**, *9* (16), 10012−10038.

(12) Talapaneni, S. N.; Hwang, T. H.; Je, S. H.; Buyukcakir, O.; Choi, J. W.; Coskun, A. Elemental-Sulfur-Mediated Facile Synthesis of a Covalent Triazine Framework for High-Performance Lithium−Sulfur Batteries. *Angew. Chem., Int. Ed.* **2016**, *55* (9), 3106−3111.

(13) Je, S. H.; Kim, H. J.; Kim, J.; Choi, J. W.; Coskun, A. Perfluoroaryl-Elemental Sulfur SNAr Chemistry in Covalent Triazine Frameworks with High Sulfur Contents for Lithium−Sulfur Batteries. *Adv. Funct. Mater.* **2017**, *27* (47), 1703947.

(14) Kim, J.; Elabd, A.; Chung, S.-Y.; Coskun, A.; Choi, J. W. Covalent Triazine Frameworks Incorporating Charged Polypyrrole Channels for High-Performance Lithium−Sulfur Batteries. *Chem. Mater.* **2020**, *32* (10), 4185−4193.

(15) Yuan, H.; Peng, H.-J.; Huang, J.-Q.; Zhang, Q. Sulfur Redox Reactions at Working Interfaces in Lithium−Sulfur Batteries: A Perspective. *Adv. Mater. Interfaces* **2019**, *6* (4), 1802046.

(16) Guo, W.; Zhang, W.; Si, Y.; Wang, D.; Fu, Y.; Manthiram, A. Artificial dual solid-electrolyte interfaces based on in situ organothiol transformation in lithium sulfur battery. *Nat. Commun.* **2021**, *12* (1), 3031.

(17) Li, Z.; Zhou, Y.; Wang, Y.; Lu, Y.-C. Solvent-Mediated Li2S Electrodeposition: A Critical Manipulator in Lithium−Sulfur Batteries. *Adv. Energy Mater.* **2019**, *9* (1), 1802207.
(18) Baek, M.; Shin, H.; Char, K.; Choi, J. W. New High Donor Electrolyte for Lithium−Sulfur Batteries. *Adv. Mater.* **2020**, *32* (52), 2005022.
(19) Shin, H.; Baek, M.; Gupta, A.; Char, K.; Manthiram, A.; Choi, J. W. Recent Progress in High Donor Electrolytes for Lithium−Sulfur Batteries. *Adv. Energy Mater.* **2020**, *10* (27), 2001456.
(20) Xu, X.; Wang, S.; Wang, H.; Xu, B.; Hu, C.; Jin, Y.; Liu, J.; Yan, H. The suppression of lithium dendrite growth in lithium sulfur batteries: A review. *J. Energy Storage* **2017**, *13*, 387−400.
(21) Gupta, A.; Bhargav, A.; Manthiram, A. Highly Solvating Electrolytes for Lithium−Sulfur Batteries. *Adv. Energy Mater.* **2019**, *9* (6), 1803096.
(22) He, Q.; Gorlin, Y.; Patel, M. U. M.; Gasteiger, H. A.; Lu, Y.-C. Unraveling the Correlation between Solvent Properties and Sulfur Redox Behavior in Lithium-Sulfur Batteries. *J. Electrochem. Soc.* **2018**, *165* (16), A4027−A4033.
(23) Cuisinier, M.; Hart, C.; Balasubramanian, M.; Garsuch, A.; Nazar, L. F. Radical or Not Radical: Revisiting Lithium−Sulfur Electrochemistry in Nonaqueous Electrolytes. *Adv. Energy Mater.* **2015**, *5* (16), 1401801.
(24) Zou, Q.; Lu, Y.-C. Solvent-Dictated Lithium Sulfur Redox Reactions: An Operando UV−vis Spectroscopic Study. *J. Phys. Chem. Lett.* **2016**, *7* (8), 1518−1525.
(25) Gupta, A.; Bhargav, A.; Manthiram, A. Evoking High-Donor-Number-Assisted and Organosulfur-Mediated Conversion in Lithium−Sulfur Batteries. *ACS Energy Lett.* **2021**, *6* (1), 224−231.
(26) Chu, H.; Jung, J.; Noh, H.; Yuk, S.; Lee, J.; Lee, J.-H.; Baek, J.; Roh, Y.; Kwon, H.; Choi, D.; et al. Unraveling the Dual Functionality of High-Donor-Number Anion in Lean-Electrolyte Lithium-Sulfur Batteries. *Adv. Energy Mater.* **2020**, *10* (21), 2000493.
(27) Chu, H.; Noh, H.; Kim, Y.-J.; Yuk, S.; Lee, J.-H.; Lee, J.; Kwack, H.; Kim, Y.; Yang, D.-K.; Kim, H.-T. Achieving three-dimensional lithium sulfide growth in lithium-sulfur batteries using high-donor-number anions. *Nat. Commun.* **2019**, *10* (1), 188.
(28) Zhu, K.; Wang, C.; Chi, Z.; Ke, F.; Yang, Y.; Wang, A.; Wang, W.; Miao, L. How Far Away Are Lithium-Sulfur Batteries From Commercialization? *Front. Energy Res.* **2019**, DOI: 10.3389/fenrg.2019.00123.
(29) Jozwiuk, A.; Berkes, B. B.; Weiß, T.; Sommer, H.; Janek, J.; Brezesinski, T. The critical role of lithium nitrate in the gas evolution of lithium−sulfur batteries. *Energy Environ. Sci.* **2016**, *9* (8), 2603−2608.
(30) Schmulbach, C. D.; Hinckley, C. C.; Wasmund, D. Solutions of alkali metals in anhydrous pyridine. *J. Am. Chem. Soc.* **1968**, *90* (24), 6600−6602.
(31) Zhou, T.; Zhao, Y.; El Kazzi, M.; Choi, J. W.; Coskun, A. Stable Solid Electrolyte Interphase Formation Induced by Monoquat-Based Anchoring in Lithium Metal Batteries. *ACS Energy Lett.* **2021**, *6* (5), 1711−1718.
(32) Xie, Z.; An, X.; Wu, Z.; Yue, X.; Wang, J.; Hao, X.; Abudula, A.; Guan, G. Fluoropyridine family: Bifunction as electrolyte solvent and additive to achieve dendrites-free lithium metal batteries. *J. Mater. Sci. Technol.* **2021**, *74*, 119−127.
(33) Xie, Z.; Wu, Z.; An, X.; Yue, X.; Yoshida, A.; Du, X.; Hao, X.; Abudula, A.; Guan, G. 2-Fluoropyridine: A novel electrolyte additive for lithium metal batteries with high areal capacity as well as high cycling stability. *Chem. Eng. J.* **2020**, *393*, 124789.
(34) Gritzner, G.; Sperker, S. Solvent donor and acceptor properties of pyridine. *J. Solution Chem.* **1990**, *19* (6), 543−553.
(35) Zheng, J.; Ji, G.; Fan, X.; Chen, J.; Li, Q.; Wang, H.; Yang, Y.; DeMella, K. C.; Raghavan, S. R.; Wang, C. High-Fluorinated Electrolytes for Li−S Batteries. *Adv. Energy Mater.* **2019**, *9* (16), 1803774.
(36) Aspern, N.; Roschenthaler, G.-V.; Winter, M.; Cekic-Laskovic, I. Fluorine and Lithium: Ideal Partners for High-Performance Rechargeable Battery Electrolytes. *Angew. Chem., Int. Ed.* **2019**, *58* (45), 15978−16000.
(37) Yoo, D.-J.; Yang, S.; Kim, K. J.; Choi, J. W. Fluorinated Aromatic Diluent for High-Performance Lithium Metal Batteries. *Angew. Chem., Int. Ed.* **2020**, *59* (35), 14869−14876.
(38) Schmeisser, M.; Illner, P.; Puchta, R.; Zahl, A.; van Eldik, R. Gutmann Donor and Acceptor Numbers for Ionic Liquids. *Chem.—Eur. J.* **2012**, *18* (35), 10969−10982.
(39) Kendall, R. A.; Dunning, T. H.; Harrison, R. J. Electron affinities of the first-row atoms revisited. Systematic basis sets and wave functions. *J. Chem. Phys.* **1992**, *96* (9), 6796−6806.
(40) Nanda, S.; Manthiram, A. Delineating the Lithium−Electrolyte Interfacial Chemistry and the Dynamics of Lithium Deposition in Lithium−Sulfur Batteries. *Adv. Energy Mater.* **2021**, *11* (11), 2003293.
(41) Zhou, T.; Zhao, Y.; El Kazzi, M.; Choi, J. W.; Coskun, A. Integrated Ring-Chain Design of a New Fluorinated Ether Solvent for High-Voltage Lithium-Metal Batteries. *Angew. Chem., Int. Ed.* **2022**, *61* (19), No. e202115884.
(42) Zhao, Y.; Zhou, T.; Ashirov, T.; Kazzi, M. E.; Cancellieri, C.; Jeurgens, L. P. H.; Choi, J. W.; Coskun, A. Fluorinated ether electrolyte with controlled solvation structure for high voltage lithium metal batteries. *Nat. Commun.* **2022**, *13* (1), 2575.
(43) Kolosnitsyn, V. S.; Kuzmina, E. V.; Karaseva, E. V.; Mochalov, S. E. A study of the electrochemical processes in lithium−sulphur cells by impedance spectroscopy. *J. Power Sources* **2011**, *196* (3), 1478−1482.
(44) Zhang, S. S.; Xu, K.; Jow, T. R. Electrochemical impedance study on the low temperature of Li-ion batteries. *Electrochim. Acta* **2004**, *49* (7), 1057−1061.
(45) Zhang, Z.; Kong, L.-L.; Liu, S.; Li, G.-R.; Gao, X.-P. A High-Efficiency Sulfur/Carbon Composite Based on 3D Graphene Nanosheet@Carbon Nanotube Matrix as Cathode for Lithium−Sulfur Battery. *Adv. Energy Mater.* **2017**, *7* (11), 1602543.
(46) Chen, H.; Zou, Q.; Liang, Z.; Liu, H.; Li, Q.; Lu, Y.-C. Sulphur-impregnated flow cathode to enable high-energy-density lithium flow batteries. *Nat. Commun.* **2015**, *6* (1), 5877.
(47) Deng, Z.; Zhang, Z.; Lai, Y.; Liu, J.; Li, J.; Liu, Y. Electrochemical Impedance Spectroscopy Study of a Lithium/Sulfur Battery: Modeling and Analysis of Capacity Fading. *J. Electrochem. Soc.* **2013**, *160* (4), A553−A558.
(48) Demir-Cakan, R.; Morcrette, M.; Gangulibabu; Guéguen, A.; Dedryvère, R.; Tarascon, J.-M. Li−S batteries: simple approaches for superior performance. *Energy Environ. Sci.* **2012**, *6* (1), 176−182.
(49) Kim, J.; Shin, H.; Yoo, D.-J.; Kang, S.; Chung, S.-Y.; Char, K.; Choi, J. W. Cobalt(II)-Centered Fluorinated Phthalocyanine-Sulfur SNAr Chemistry for Robust Lithium−Sulfur Batteries with Superior Conversion Kinetics. *Adv. Funct. Mater.* **2021**, *31* (51), 2106679.
(50) Li, B.-Q.; Kong, L.; Zhao, C.-X.; Jin, Q.; Chen, X.; Peng, H.-J.; Qin, J.-L.; Chen, J.-X.; Yuan, H.; Zhang, Q.; et al. Expediting redox kinetics of sulfur species by atomic-scale electrocatalysts in lithium−sulfur batteries. *InfoMat* **2019**, *1* (4), 533−541.
(51) Fan, F. Y.; Chiang, Y.-M. Electrodeposition Kinetics in Li-S Batteries: Effects of Low Electrolyte/Sulfur Ratios and Deposition Surface Composition. *J. Electrochem. Soc.* **2017**, *164* (4), A917−A922.

https://doi.org/10.1021/acsenergylett.2c00874
ACS Energy Lett. XXXX, XXX, XXX−XXX